NASA Technical Memorandum 102528
ICOMP-90-08

Three-Dimensional Euler Time Accurate Simulations of Fan Rotor-Stator Interactions

A.A. Boretti
Centro Ricerche FIAT—MOTORI
Orbassano, Italy

and Institute for Computational Mechanics in Propulsion
Lewis Research Center
Cleveland, Ohio

December 1990

NASA

THREE-DIMENSIONAL EULER TIME ACCURATE SIMULATIONS OF FAN ROTOR-STATOR INTERACTIONS

A.A. Boretti
Centro Richerche FIAT - MOTORI
Orbassano, Italy

and Institute for Computational Mechanics in Propulsion*
Lewis Research Center
Cleveland, Ohio 44135

SUMMARY

The paper presents a numerical method useful to describe unsteady three-dimensional flow fields within turbomachinery stages. The method solves the compressible, time-dependent, Euler conservation equations with a finite-volume, flux-splitting, total-variation-diminishing, approximately factored, implicit scheme. Multiblock composite gridding is used to partition the flow field into a specified arrangement of blocks with static and dynamic interfaces. The code is optimized to take full advantage of the processing power and speed of the Cray Y/MP supercomputer. The method is applied to the computation of the flow field within a single-stage, axial flow fan, thus reproducing the unsteady three-dimensional rotor-stator interaction.

NOMENCLATURE

A,B,C	quasi-linear matrices
a_j	strength of j^{th} wave
$b^{(j)}$	speed of j^{th} wave
E	total internal energy
e	internal energy
F,G,H	flux vectors
f	unknown vector
H	total enthalpy
h	enthalpy
IB	leading edge i index
IE	trailing edge i index
i,j,k	space discretization indices
J	Jacobian
L_j	limiter
$l^{(j)}$	left eigenvector
M	Mach number
m	plane index

*Work funded by Space Act Agreement C-99066-G.

NI	maximum block i count
NJ	maximum block j count
NK	maximum block k count
p	pressure
$\mathbf{r}^{(j)}$	right eigenvector
T	residual vector
t	time
U,V,W	contravariant velocity components
u,v,w	velocity components
x,y,z	Cartesian coordinates
α	specific heat ratio
β,ε	limiter parameters
Γ,Ω,Π	curvilinear coordinates
δt	time step
δx	mesh size
θ,ϕ	time discretization parameter
Σ^+	summation over positive wave speeds
Σ^-	summation over negative wave speeds
σ	density
Φ	space discretization parameter

Subscripts:

l	left
r	right

Superscript:

n	time level

INTRODUCTION

The numerical methods for the simulation of single-domain, steady, three-dimensional flow fields developed over the past years are now widely used within a design environment. These methods include both Euler (Denton 1983; Van Hove 1983) and Navier-Stokes (Dawes 1986 a,b, 1987; Hah 1984, 1986; Shamroth et al. 1982; Roscoe et al. 1984; Weinberg et al. 1986; and Moore 1985) solvers. Although the Navier-Stokes methods can produce better computational results, their use as a design tool appears to be certainly more difficult, due to the increased number of parameters influencing the solution accuracy. Analyses of flows through isolated rows can be used to study many of the aerodynamic phenomena in turbomachinery, but such analyses yield no information regarding the unsteadiness arising from the interaction of rotating and stationary blade rows.

Since the flow within a turbomachine is extremely complex, computational methods can be used to great advantage in understanding such flows. An accurate analysis of the flow associated with rotating and stationary row configurations can be very helpful in optimizing the performance of the whole turbomachine. Within each stage, rotor and stator rows alternate and thus produce particularly strong interactions. As shown by Dring et al. (1982), the temporal pressure fluctuation near the leading edge of the rotor can be as much as 72 percent of the exit dynamic pressure in a rotor-stator interaction problem with a 15-percent chord length axial gap. Numerical methods to simulate multidomain, unsteady, three-dimensional flow fields appear therefore to be particularly interesting. The present paper describes the development of one of these new numerical methods.

The simulation of the rotor-stator interaction problem needs the introduction of a particularly complex flow model. The problem is assumed to be governed by the three-dimensional Euler conservation equations, written in unsteady, compressible form, with the gas density, velocity, and energy as the basic variables. These equations have to be solved in a particularly complex flow domain. Multi-blade-passage and multi-blade-row configurations have to be considered to simulate the unsteady rotor-stator interaction. Turbomachinery bladings are usually highly skewed, and the hub and tip surfaces strongly diverge. Moreover, fixed and movable blade passages alternate. As a result, both fixed and movable blade passages are bounded by strongly irregular surfaces, and information must be transferred from a fixed to a movable reference frame. Furthermore, high flow resolution in both space and time is required. Finally, the unsteady flow behavior requires the proper treatment of boundary conditions.

The development of a numerical method resolving the flow model previously described poses many programming problems. The equations have to be solved in a time-dependent, body-fitted, curvilinear, reference frame. The discretization of a flow domain including multi-blade-passages and multi-blade-rows requires the introduction of multiblock gridding, where the whole flow domain is partitioned in a specified arrangement of blocks. These blocks are limited by the boundaries of the flow domain or by block interfaces. The high resolution in space requires, in addition to the introduction of a proper grid refinement where higher flow gradients are expected to occur, a proper selection of block arrangements and individual block dimensions. The use of a finite-volume space discretization, with an accurate flux-corrected interface flux-splitting formula and a total-variation-diminishing approach in limiting the components of the interface flux, produces high spatial accuracy. A multistep, approximately factored, implicit scheme produces high time accuracy. Multiblock gridding with static and dynamic grid interfaces is used to properly discretize the complex flow field. The relative motion of rotor and stator blades is simulated by using grids that move relative to each other, with proper treatment at the interface between blade rows. The implementation of appropriate boundary conditions is based on characteristic concepts. A characteristic variable boundary condition technique is introduced in the time-dependent, body-fitted reference frame for inflow, outflow, and solid boundaries, and it is implemented by using phantom cells.

The method is used to model the unsteady flow in a single-stage, transonic, axial flow fan. The test case considered here does not exhibit such a particularly strong interaction as that shown in the work of Dring et al. (1982). The rotor and stator are separated by approximately 85-percent rotor chord at midspan, thus reducing (but not eliminating) the flow field interactions between blade rows. The computational domain is made up of two rotor blade passages, each discretized by using about 13 500 grid points, and three stator blade passages, each discretized by using 8500 grid points. The total number of grid points involved in the rotor-stator

problem discretization therefore equals 52 500. Approximately 190 vital pieces of information have to be known for each cell. The computations have been performed on the NASA Ames Cray Y/MP computer. At the beginning of the computations, the rotor-stator interface orientation is defined with the rotor-blade trailing edges located midway between the neighboring stator-blade leading edges. The user CPU time required for each rotor-stator orientation is about 700 sec. The system CPU time is about 150 sec. The internal memory required is only 2 megawords. The result obtained after four interface reorientations are presented and compared with laser anemometer measurements for both rotor (Pierzga and Wood 1985) and stator (Suder et al. 1987; and Hathaway et al. 1987) rows. The theoretical results are also compared with other steady-state theoretical results. These comparisons allow a first assessment of the code prediction capability.

EULER FLOW MODEL

The computation of high Reynolds number, unseparated, unsteady cascade flow fields can easily be accomplished by solving the Euler conservation equations, written in unsteady, compressible form. The basic variables are the gas density, velocity, and energy. Their conservation equations are written in a body-fitted, time-dependent, curvilinear, reference frame:

$$\Gamma = \Gamma(x,y,z,t)$$

$$\Omega = \Omega(x,y,z,t)$$

$$\Pi = \Pi(x,y,z,t)$$

In vector form,

$$f_{,t} + \mathbf{F}_{,\Gamma} + \mathbf{G}_{,\Omega} + \mathbf{H}_{,\Pi} = 0$$

where

$$\mathbf{f} = (\sigma,\ \sigma u,\ \sigma v,\ \sigma w,\ \sigma E)^t$$

$$\mathbf{F} = (\sigma,\ \sigma uU + p\Gamma_{,x},\ \sigma vU + p\Gamma_{,y},\ \sigma wU + p\Gamma_{,z},\ \sigma Uh - p\Gamma_{,t})^t$$

$$\mathbf{G} = (\sigma,\ \sigma uV + p\Omega_{,x},\ \sigma vV + p\Omega_{,y},\ \sigma wV + p\Omega_{,z},\ \sigma Vh - p\Omega_{,t})^t$$

$$\mathbf{H} = (\sigma,\ \sigma uW + p\Pi_{,x},\ \sigma vW + p\Pi_{,y},\ \sigma wW + p\Pi_{,z},\ \sigma Wh - p\Pi_{,t})^t$$

$$p = (\alpha - 1)/\alpha\sigma h = (\alpha - 1)\sigma e$$

$$h = H - (u^2 + v^2 + w^2)/2$$

$$e = E - (u^2 + v^2 + w^2)/2$$

The Jacobian J, the metric quantities $\Gamma_{,x}$, $\Gamma_{,y}$, $\Gamma_{,z}$, $\Gamma_{,t}$, $\Omega_{,x}$, $\Omega_{,y}$, $\Omega_{,z}$, $\Omega_{,t}$, $\Pi_{,x}$, $\Pi_{,y}$, $\Pi_{,z}$, and $\Pi_{,t}$, and the contravariant velocities U, V, and W are given in appendix A.

The integration requires the introduction of the conditions to be fulfilled along the boundaries of the domain of interest. The physical flow domain is limited by inflow, outflow, solid, and periodic boundaries where appropriate boundary conditions are needed. The boundary conditions along inflow, outflow, and solid boundaries are defined according to characteristic concepts - i.e., by discretizing the flow equations written in characteristic form, thus simulating the correct unsteady

flow behavior. Before starting the time integration, proper initial conditions have to be specified. These conditions can be either a previously computed steady-state condition or a rough approximation of a steady flow condition.

NUMERICAL METHOD

The integration of the Euler equations, over discrete contiguous volumes, in a computational space where $\delta X=\delta Y=\delta Z=1$, yields for the grid point i,j,k the following cell-centered finite-volume formula:

$$\mathbf{f}_{,t} = -\delta_i \mathbf{F} - \delta_j \mathbf{G} - \delta_k \mathbf{H}$$

where

$$\delta_i \mathbf{F} = \mathbf{F}_{i+1/2} - \mathbf{F}_{i-1/2}$$

$$\delta_j \mathbf{G} = \mathbf{G}_{j+1/2} - \mathbf{G}_{j-1/2}$$

$$\delta_k \mathbf{H} = \mathbf{H}_{k+1/2} - \mathbf{H}_{k-1/2}$$

The dependent variable vector $\mathbf{f}$ represents values at the cell centers, while the vector flux functions $\mathbf{F}(\mathbf{f})$, $\mathbf{G}(\mathbf{f})$, and $\mathbf{H}(\mathbf{f})$ represent values at the interface between neighboring cells. The evaluation of the vector flux functions at the cell interfaces is performed by using the values in the neighboring cells. The interface terms are computed according to a one-parameter flux-difference-splitting scheme.

For ease of understanding, the flux-difference-splitting scheme is presented here in one space dimension. As reported in appendix B, a family of high spatial accuracy formulae is written as follows:

$$\mathbf{F}^{\wedge}_{i+1/2} = \mathbf{F}_{i+1/2} + (1+\Phi)/4\left(d\mathbf{F}^{+}_{i+1/2} - d\mathbf{F}^{-}_{i+1/2}\right) + (1-\Phi)/4\left(d\mathbf{F}^{+}_{i-1/2} - d\mathbf{F}^{-}_{i+3/2}\right)$$

where $d\mathbf{F}$ is the interface flux difference for the collection of waves. The superscript denotes either positive or negative traveling waves. The option $\Phi=1/3$ gives a third-order accurate scheme; the option $\Phi=-1$ gives a fully upwind second-order accurate scheme. These one-dimensional formulae can be extended to three dimensions by assuming that all waves travel normal to their respective interfaces.

Spurious oscillations are controlled by using total-variation-diminishing concepts in limiting the components of the interface flux. The use of limiters yields the following expressions for the corrective flux terms:

$$d\mathbf{F}^{+}_{i+1/2} = \Sigma^{+} L_j(1,-1)\mathbf{r}^{(j)}_{i+1/2}$$

$$d\mathbf{F}^{+}_{i-1/2} = \Sigma^{+} L_j(-1,1)\mathbf{r}^{(j)}_{i+1/2}$$

$$d\mathbf{F}^{-}_{i+1/2} = \Sigma^{-} L_j(1,3)\mathbf{r}^{(j)}_{i+1/2}$$

$$d\mathbf{F}^{-}_{i+3/2} = \Sigma^{-} L_j(3,1)\mathbf{r}^{(j)}_{i+1/2}$$

where $\mathbf{r}^{(j)}$ is a right eigenvector of the quasi-linear matrix $\mathbf{A}=\mathbf{F}_{,f}$. Different limiter expressions have been proposed. These expressions are presented in appendix C.

The previous equations are finally integrated in time by using an approximately factored, implicit scheme. The equation is first written in the linearized, discrete, integral delta form

$$[I + \theta\delta t/(1 + \phi)\mathbf{M}^n*]\cdot\delta\mathbf{f}^n = -\delta t/(1 + \phi)\mathbf{T}^n + \phi/(1 + \phi)\delta\mathbf{f}^{n-1}$$

Different members of this family have particular relevance. If θ=1 and ϕ=1/2, the scheme is three-point backward; if θ=1 and ϕ=0, it is backward Euler; and if θ=1/2 and ϕ=0, it is trapezoidal. The left side of the previous time-stepping formula is expressed as follows:

$$\mathbf{M}^n* = \delta_i\mathbf{A}^+* + \delta_i\mathbf{A}^-* + \delta_j\mathbf{B}^+* + \delta_j\mathbf{B}^-* + \delta_k\mathbf{C}^+* + \delta_k\mathbf{C}^-*$$

where

$$\mathbf{A}^{+(-)} = (\mathbf{F}^{+(-)}{}_{,f})^n$$

$$\mathbf{B}^{+(-)} = (\mathbf{G}^{+(-)}{}_{,f})^n$$

$$\mathbf{C}^{+(-)} = (\mathbf{H}^{+(-)}{}_{,f})^n$$

with $\mathbf{F}^{+(-)}$, $\mathbf{G}^{+(-)}$, and $\mathbf{H}^{+(-)}$ resulting from flux-vector-splitting theory (Steger and Warming, 1981) while the right side is expressed as

$$\mathbf{T}^n = \delta_i\mathbf{F}^n + \delta_j\mathbf{G}^n + \delta_k\mathbf{H}^n$$

with $\mathbf{F}$, $\mathbf{G}$, and $\mathbf{H}$ resulting from the flux-difference-splitting theory discussed herein (for further details, see Janus 1989).

For ease of computer programming, the left side operator is split into the product of two operators:

$$[\mathbf{I} + \theta\delta t/(1 + \phi)\mathbf{M}^+*]\cdot\delta\mathbf{f}\hat{} = -\delta t/(1 + \phi)\mathbf{T}^n + \phi/(1 + \phi)\delta\mathbf{f}^{n-1}$$

$$[\mathbf{I} + \theta\delta t/(1 + \phi)\mathbf{M}^-*]\cdot\delta\mathbf{f}^n = \delta\mathbf{f}\hat{}$$

$$\mathbf{f}^{n+1} = \mathbf{f}^n + \delta\mathbf{f}^n$$

In the solution procedure, since the first operator is applied by moving forward, it is referred to as the forward operator. The second one is applied by moving backward and therefore is referred to as the backward operator. The left side operators are defined as follows:

$$\mathbf{M}^{+(-)}* = \delta_i\mathbf{A}^{+(-)}* + \delta_j\mathbf{B}^{+(-)}* + \delta_k\mathbf{C}^{+(-)}*$$

Despite factoring, the scheme seems to retain the original unconditional stability.

The implementation of appropriate boundary conditions is based on characteristic concepts. A characteristic variable boundary condition technique is introduced in a time-dependent body-fitted reference frame for inflow, outflow, and solid boundaries (Whitfield and Janus 1989). These boundary conditions are implemented by using phantom cells, with changes in dependent variables $\delta\mathbf{f}^n$ and $\delta\mathbf{f}*$ to be set equal to zero in these phantom cells. It is pointed out that the outflow boundary condition uses both the characteristic variable form of the equations and a radial equilibrium

condition where the outflow static pressure at the hub is specified. Better details on the numerical method can be found in Janus (1989).

COMPUTER CODE

The code was written (Whitfield and Janus 1989) and further optimized for use on the NASA Ames Cray Y/MP computer. The Cray Y/MP has 8 processors, 32 megawords of common memory and 256 megawords of solid-state storage, and it allows particularly efficient computational fluid-dynamic simulations, especially when some guidelines are followed in the code development.

Because of the in-core memory limitations associated with the computation of complex three-dimensional flow fields, the overall flow environment is segmented into several smaller and more manageable intercommunicating flow environments. Figure 1 shows the composite field circumferential and axial partitioning. The global domain is first circumferentially partitioned by considering different blade passages. The domain is then axial partitioned by considering different blade rows. Each blade row is granted limited rotational freedom relative to the adjacent blade rows. When the domain is completely partitioned, a block referencing scheme is introduced following the global axes orientation. Within each block, the local axes are assumed to follow the global axes. The block index limits NI, NJ, and NK are restricted such that for all blocks within a blade row NI, NJ, and NK remain constant. In addition, NJ remains constant between blade rows. Variations in NI are permitted between blade rows. Variations in NK are permitted between blade rows in the limits of a constant circumferential cell count (the product of NK by the number of circumferential blocks) to be satisfied.

The reduction of in-core (primary) memory requirements calls for the use of secondary memory, in particular for the use of the Cray's rapid access solid-state storage device (SSD). The use of computational blocks of differing cell count, and therefore differing memory requirements, complicates memory utilization. The ribbon vector dynamic memory management (Janus 1989) stores the entire field on secondary memory with the exception of the block currently under execution. The method allows the adjustment of the in-core field length to accommodate each block, regardless of size, without excess memory words.

The optimization of the processing of the data residing in memory calls for a reduction of IO wait time. Unblocked data transmission to and from secondary memory is used. All data contained within the ribbon vector are transferred between in-core and secondary memory via unblocked standard FORTRAN I/O statements. Proper unblocked data length has to be provided.

Vectorizing FORTRAN compilers identify inner DO loops that are suitable for vectorization. Since this enables the loop to run in vector mode, the program runs much faster. It is important to note that if a loop has even one nonvectorizble construct the entire loop will not be vectorized. There are a number of constructs that can decrease the performance of a code. The process of optimization of a code to obtain peak performance on the Cray Y/MP can be regarded as the elimination of these constructs. Some general vectorizing guidelines are provided for this purpose. The constructs that can decrease the performance of a code are usually referred to as memory strides, vector lengths, vector dependencies and recursions, logically separate vectors within a single array, loops with IF statements, loops with subroutines, and functions calls.

The term stride refers to the increment in memory between successive words fetched or stored in a vector operation. Bad strides can cause the code to run significantly slower. The vector length of an operation is the number of times an inner DO loop is executed. Longer vectors are processed more efficiently. DO loops cannot be vectorized in cases where calculations for one iteration of a loop require results from a previous iteration (vector dependency). Loops that reference independent sections of a single array can often appear to have vector dependencies. IF statements prevent loops from being vectorized. Subroutine and function calls prevent vectorization for many reasons.

The code development has to include some general guidelines. Vectors have to be thought of as fundamental constructs. Vector operations have to be isolated from scalar operations. Control statements have to be avoided in loops. Recursion has to be avoided or moved to outer loops. Power-of-two memory strides have to be avoided. The array subscripts have to be kept simple and explicit. In nested DO loops, the inner DO loop has to be made as long as possible. Double precision has to be avoided unless absolutely necessary. Floating-point arithmetic operations have to be used instead of integer arithmetic operations (except in array subscripts). System library routines have to be used when possible.

In the cases of loops that reference independent sections of a single array, indexing techniques should be used to define two logical arrays within a single physical array. There are many approaches to vectorizing loops with IF statements. The method called loop splitting divides a loop into its vectorizable and nonvectorizable parts. The loop restructuring removes redundant IF statements or restructures loops with invariant IF statement. The approaches to vectorizing loops with subroutine calls include using statement functions, promoting the subroutine into the loop, or expanding the subroutine to include the loop.

The adopted approximately factored, implicit scheme poses a problem of vector dependency. The implicit scheme involves point simultaneous solutions and backward or forward substitutions, and it poses a problem of vector dependency during the substitution. To circumvent this, a procedure simultaneously processing those cells lying on a special diagonal plane in the computational space is introduced. Cells whose indices satisfy the equation of the diagonal plane, expressed as $i+j+k=m$, where m is a constant designating the plane level, are computationally independent. Diagonal plane processing can then be used with the aid of indirect addressing to facilitate the vectorization of a backward or forward substitution.

The advance of the flow field in time requires two global sweeps through the global domain, one forward and one backward. In addition, all blocks are forward swept internally and then they are backward swept internally. An equivalence to the analogous single-block solution is thus provided. The internal forward sweep within each block consists of operating on each cell on a diagonal plane, from the lowest level interior plane to the highest level interior plane, by applying the forward operator at each computational cell. After information due to communication has been collected, the in-core resident block is returned to secondary memory and the next block is transferred in-core. The internal backward sweep is similar, although the planes are traversing in decreasing rather than in increasing order, and the operator applied is the backward one.

The communication between blocks is accomplished by considering continuous grid lines between blocks. Values from within the domain of one block are extracted and then injected as phantom values in an adjacent block. Since each blade row can rotate relative to its adjacent blade rows, continuous grid lines are required across

the shearing block-block interface at all time levels. The shearing block-block interface in physical space yields a dynamic interface in computational space, with a progressive changing of communication partners. The block-block communication is properly accomplished by simulating the internal cell communication within the blocks. The implementation of boundary conditions as well as the transfer between neighboring blocks is implemented by using phantom cells. This approach wastes a small amount of memory for the offset, fully justified by the simplification of the problem. Other details about the computer codes can be found in Janus (1989).

RESULTS

The code has been applied to the computation of the flow in a single-stage, transonic, axial-flow fan. Figure 2 shows the plane view of the single-stage fan flow path (Hathaway 1986). Figure 3 shows the representative rotor blade sections at three spanwise locations, hub, midspan, and tip. Figure 4 shows the representative stator blade sections at three spanwise locations, hub, midspan, and tip. The design speed of the fan is 16 043 rpm and the corrected mass flow rate is 34 kg/s. The rotor and stator are separated by approximately 85-percent rotor chord at midspan. The advantage of the wide axial spacing between blade rows is that the flow field interactions between the blade rows are reduced, thus decreasing the fan noise.

The rotor is composed of 22 blades of multiple-circular-arc design. The rotor aspect ratio (averaged) is 1.550. The inlet tip diameter is 51.3 cm; the inlet hub/tip radius ratio is 0.375; and the rotor tip clearance is 0.5 mm. The stator is composed of 34 blades of double-circular-arc design. The stator discharges the fluid axially. The axial chord is a constant 5.6 cm from hub to tip. The tip diameter is constant at 48.7 cm. The inlet hub/tip radius ratio is 0.500, while the exit hub/tip radius ratio is 0.530.

Some unsteady experimental results (Hathaway et al. 1987) are presented in figure 5. The dominant blade-row interactions are due to viscous interactions caused by the chopping of rotor wakes by the downstream stator blade row. The figure shows a sequence of plots of the turbulence kinetic energy contours, for a rotor rotation of one pitch, at midspan. SP denotes rotor shaft position: 50 rotor shaft positions are specified per rotor pitch. The shaded regions identify rotor wake fluid. After the stator blade chops the rotor wake, the wake segments move at different speeds along the stator blade pressure and suction sides. When the rotor wake segments reach the stator exit, there is a drift between the rotor wake segments originally part of the same rotor wake.

Calculations have been performed by considering two rotor and three stator blade row blocks. Each rotor blade row block is made up of NIxNJxNK grid points, with NI=49 planes from inlet to exit, NJ=21 planes from hub to tip, and NK=13 planes from suction to pressure side. The leading edge is located at IB=21, while the trailing edge is located at IE=41. Each stator blade row block is made up of NI=45 planes from inlet to exit, NJ=21 planes from hub to tip, and NK=9 planes from suction to pressure side. The leading edge is located at IB=9, while the trailing edge is located at IE=21. The last five rotor axial planes and the first five stator axial planes are used for communication between blade rows. The rotor and stator blade passage computational grids are shown in figure 6.

Calculations are started from a rough approximation of the flow field and the flow equations are then integrated in time. The selected code options allow second-order accuracy in time and third-order accuracy in space. The limiter adopted is the

van Leer limiter. The relative motion between blade rows requires 264 time cycles for each interface reorientation. The computations have been performed on the NASA Ames Cray Y/MP computer. The user CPU time required for each interface reorientation is about 700 sec, while the system CPU time is about 150 sec. The internal memory required in only 2 megawords.

The upstream boundary conditions are specified in terms of a free stream Mach number, taken equal to 0.5565, and free stream flow angles, defining an inlet axial direction. The downstream boundary condition is specified in terms of a hub static pressure, fixed at 1.7869 times the inlet static pressure. These boundary conditions simulate the real flow conditions with some difficulties. For many reasons, the correct mass flow rate is not perfectly verified. The mass flow rates experimentally measured have a relatively strong degree of uncertainty. Many runs are required to establish the proper boundary conditions to obtain a prefixed value in the mass flow. Most of the results available for the rotor have been obtained without a downstream stator row. Finally, it is well known that the best agreement with experimental data in computing flows within compressors or fans requires the evaluation of viscous effects (Pierzga and Wood 1985). For all these reasons, the boundary conditions have been defined on the basis of simple one-dimensional concepts, without running the code, and the correct mass flow rate is therefore not verified in the calculations.

The three-dimensional rotor-stator interaction simulation provides the user a huge amount of information. In a first stage of validation, only the results obtained for a particular rotor shaft position are considered. The results obtained after four interface reorientations are presented and compared with laser anemometer measurements for both rotor (Pierzga and Wood 1985) and stator rows (Hathaway et al. 1987). These comparisons allow the user to assess the prediction capability of the Euler code not only from a qualitative but from a quantitative viewpoint.

Figure 7 to 16 show some computational results obtained for the rotor row, compared with available experimental data and other computational results, obtained using Denton's code (Denton 1983). The experimental results were obtained with a laser anemometer for a rotor row without a downstream stator row (Pierzga and Wood 1985). Denton's Euler code, modified to include the effects of boundary layer displacement (in order to obtain the best agreement with experimental data), was applied to the test case defined in the experiments (Pierzga and Wood 1985).

Figure 7 shows (from left to right) the relative Mach number contours in the rotor row leading edge, trailing edge, and exit planes. The rotor flow appears to be strongly three-dimensional and rotational.

Figure 8 shows the relative Mach number contour results obtained with the laser anemometer (left) and Denton's code (right) at 30-percent span from the tip. Figure 9 shows the present computational results for the same flow surface. The relative inlet Mach number is supersonic. The shock location is shown to provide a clearer picture of the flow in the passage. The shock location was determined by considering the Mach number and flow angle data in the streamwise direction and by assuming the starting point of the flow deceleration as the shock front (Pierzga and Wood 1985). The agreement between data is quite good, with only minor differences. A normal shock is followed by a second shock. The peak Mach number ahead of the first shock is about 1.4. This shock is accurately located by the present code with a peak Mach number of about 1.375. The second shock is shown extending from the pressure surface to about midpitch, while closer to the suction surface, the location of the shock is more difficult to determine. The location and the extension of this second shock is the major difference between the experiment and the analysis. The

computed Mach number in the rear part of the blade is only slightly lower than the measured one, 0.85 compared to 0.90. The numerical calculations produce shocks that are smeared over several grid points, probably due to grid coarseness and neglected viscous effects. The code prediction capability appears to be quite good, especially when compared with the accuracy provided by Denton's code, certainly more calibrated on the specific test case. There is a higher static pressure downstream of the rotor blade row that reduces the flow velocities in the rear part of the blade passage.

A more quantitative comparison between experimental and theoretical data is the blade surface velocity comparison. The blade surface velocity data predictions are the most important in helping the designer tailor the blade shape. Figure 10 shows the comparison between experimental and theoretical results for the relative Mach number differences between pressure and suction side at 30-percent span from the tip. The laser anemometer data are taken at the first point off the blade surface, close to 5- and 95-percent pitch, and therefore the computational results are selected at the same locations. The agreement appears to be quite satisfactory in both the suction and pressure side velocities, with only minor changes in the values on the rear blade surfaces.

Figure 11 shows the relative Mach number contour results obtained with the laser anemometer (left) and Denton's code (right) at 10-percent span from the tip. Figure 12 shows the present computational results for the same flow surface. The relative inlet Mach number is increasingly supersonic with reference to the value in the section at 30-percent span from the tip. The agreement between data is particularly good. The presence of a second shock is not clearly evident. The peak Mach number ahead of the first shock is about 1.4. The shock is accurately located by the present code with a peak Mach number of about 1.375. The computed Mach number in the rear part of the blade is now lower than the measured one, 0.875 compared to 0.975, but the code prediction capability appears to be quite satisfactory, within the limits of accuracy obtained in a solution of the Euler equations.

Figure 13 shows a comparison between experimental and theoretical results for the relative Mach number differences between pressure and suction side at 10-percent span from the tip. The agreement appears to be better than that obtained on the flow surface at 30-percent span from the tip. Minor differences in the values on the rear blade surfaces still remain.

Figure 14 shows the relative Mach number contour results obtained with the laser anemometer (left) and Denton's code (right) at 70-percent span from the tip. Figure 15 shows the present computational results for the same flow surface. The relative inlet Mach number is now subsonic. The peak Mach number close to the blade leading edge is lower than that in the experiments, as well as the rear flow Mach number, especially close to the blade pressure side. The mass flow close to the hub seems to be strongly reduced with reference to the value obtained in the experiments. Finally, figure 16 shows the comparison between experimental and theoretical results for the relative Mach number differences between pressure and suction sides at 70-percent span from the tip. The agreement appears to be worse than that obtained on the flow surfaces at 10- and 30-percent spans from the tip, and there are strong differences in surface velocities especially on the blade pressure side.

Most of the differences between experimental and computational results seem to be due to the influence of the downstream stator row on the rotor flow field. The flow picture provided by the Euler flow model certainly appears to be better than expected.

While experimental data are available in enough detail for the rotor flow (but these results do not consider a downstream stator row), only a few experimental data have been provided for the stator row. Despite this, these results have a particular significance since they have been obtained by considering an upstream rotor row.

Figures 17 to 19 show some computational results obtained for the stator row. Figure 17 shows (from left to right) the Mach number contours in the stator row inlet, leading edge, and trailing edge planes. The stator flow appears to be strongly three-dimensional and rotational from the inlet plane. Figure 18 shows the Mach number contour results obtained with the laser anemometer (Hathaway et al. 1987) at 50-percent span from the tip. Figure 19 shows the present computational results for the same flow surface. The inlet Mach number is subsonic. The agreement between data is quite good. The peak Mach number on the suction side is predicted fairly well, with a very similar 0.70 constant Mach number contour. The same is true for the Mach number in the rear part of the blade, with only minor underestimation, 0.55 compared to 0.59.

The relative influence of stator and rotor rows appears to be well simulated.

CONCLUSIONS

This paper has presented a computer code developed for the analysis of unsteady three-dimensional flow fields within turbomachine stages. The model takes into account the unsteady flow fields within complex domains including multi-blade-passage and multi-blade-row (both fixed and movable) configurations. The flow model has a particularly wide generality and is thus applicable to the solution of the majority of problems arising in the aerodynamic and acoustic design of turbomachinery components.

The multiblock gridding allows one to properly discretize the multi-blade-passages and multi-blade-row configurations. The partitioning of the whole flow domain in a specified arrangement of blocks is the only answer to discretize flow domains requiring a huge number of grid points with strongly varying grid refinements. The block interface treatment probably requires further work to improve the transfer of information without introducing interface errors.

The finite-volume, flux-corrected interface flux-splitting, total-variation-diminishing space discretization allows up to third-order accurate space discretizations without undesired artificial viscosity. The multistep, approximately factored, implicit time discretization shows an apparently unconditional stability and produces up to second-order accuracy in time. Finally, the efficient use of the hardware capability of the Cray Y/MP supercomputer leads to significantly reduced costs of very complex fluid-dynamic simulation.

ACKNOWLEDGMENTS

The author would like to express his indebtedness to NASA Lewis Research Center, Cleveland, Ohio, and in particular to Dr. L. Povinelli, for support of this research activity. The author would also like to acknowledge Dr. Jose Sanz for support in the use of the NASA Ames Numerical Aerodynamic Simulation Program Processing System Network, introduction to the code structure, and suggestions in the code modifications. Finally, the author wishes to express his appreciation to Dr. D. Whitfield and Dr. M. Janus of Mississippi State University for their assistance and permission to use their code in the computations.

APPENDIX A - COORDINATE TRANSFORMATION

The Euler conservation equations are written in a body-fitted, time-dependent, curvilinear, reference frame. The coordinate transformation

$$\Gamma = \Gamma(x,y,z,t)$$

$$\Omega = \Omega(x,y,z,t)$$

$$\Theta = \Theta(x,y,z,t)$$

leads to the following Jacobian and metric quantities expression:

$$J = x_{,\Gamma}(y_{,\Omega}z_{,\Theta} - z_{,\Omega}y_{,\Theta}) - y_{,\Gamma}(x_{,\Omega}z_{,\Theta} - z_{,\Omega}x_{,\Theta}) + z_{,\Gamma}(x_{,\Omega}y_{,\Theta} - y_{,\Omega}x_{,\Theta})$$

$$\Gamma_{,x} = J^{-1}(y_{,\Omega}z_{,\Theta} - z_{,\Omega}y_{,\Theta})$$

$$\Gamma_{,y} = J^{-1}(z_{,\Omega}x_{,\Theta} - x_{,\Omega}z_{,\Theta})$$

$$\Gamma_{,z} = J^{-1}(x_{,\Omega}y_{,\Theta} - y_{,\Omega}x_{,\Theta})$$

$$\Gamma_{,t} = -x_{,t}\Gamma_{,x} - y_{,t}\Gamma_{,y} - z_{,t}\Gamma_{,z}$$

$$\Omega_{,x} = J^{-1}(y_{,\Theta}z_{,\Gamma} - y_{,\Gamma}z_{,\Theta})$$

$$\Omega_{,y} = J^{-1}(x_{,\Gamma}z_{,\Theta} - z_{,\Gamma}x_{,\Theta})$$

$$\Omega_{,z} = J^{-1}(x_{,\Theta}y_{,\Gamma} - y_{,\Theta}x_{,\Gamma})$$

$$\Omega_{,t} = -x_{,t}\Omega_{,x} - y_{,t}\Omega_{,y} - z_{,t}\Omega_{,z}$$

$$\Theta_{,x} = J^{-1}(y_{,\Gamma}z_{,\Omega} - z_{,\Gamma}y_{,\Omega})$$

$$\Theta_{,y} = J^{-1}(x_{,\Omega}z_{,\Gamma} - z_{,\Omega}y_{,\Gamma})$$

$$\Theta_{,z} = J^{-1}(x_{,\Gamma}y_{,\Omega} - y_{,\Gamma}x_{,\Omega})$$

$$\Theta_{,t} = -x_{,t}\Theta_{,x} - y_{,t}\Theta_{,y} - z_{,t}\Theta_{,z}$$

The contravariant velocities are given as follows:

$$U = \Gamma_{,x}u + \Gamma_{,y}v + \Gamma_{,z}w + \Gamma_{,t}$$

$$V = \Omega_{,x}u + \Omega_{,y}v + \Omega_{,z}w + \Omega_{,t}$$

$$W = \Theta_{,x}u + \Theta_{,y}v + \Theta_{,z}w + \Theta_{,t}$$

APPENDIX B - FLUX-DIFFERENCE-SPLITTING FORMULAE

The evaluation of the vector flux functions at the cell interfaces is performed by using the values in the neighboring cells according to a one-parameter flux-difference-splitting scheme. For ease of understanding, the scheme is presented here in one space dimension. The flux difference at the interface between left and right cells is expressed as

$$d\mathbf{F} = \mathbf{F}_r - \mathbf{F}_l = \mathbf{A}(\mathbf{f}_r - \mathbf{f}_l) = \mathbf{A}\cdot d\mathbf{f}$$

where $\mathbf{A}=\mathbf{F}_{,f}$ is s quasi-linear matrix, representative of local interface. The matrix $\mathbf{A}$ is evaluated at the interface according to the Roe averaging procedure (Roe et al. 1984) by using the following relations:

$$\sigma = (\sigma_l \sigma_r)^{1/2}$$

$$u = (\sigma_l^{1/2} u_l + \sigma_r^{1/2} u_r)/(\sigma_l^{1/2} + \sigma_r^{1/2})$$

$$H = (\sigma_l^{1/2} H_l + \sigma_r^{1/2} H_r)/(\sigma_l^{1/2} + \sigma_r^{1/2})$$

Each set of left or right eigenvectors forms a spanning set in state space, and a basis is constructed using these orthonormal vectors. The interface differential $d\mathbf{f}$ is thus proportional to the right eigenvectors $\mathbf{r}^{(j)}$ of $\mathbf{A}$:

$$d\mathbf{f} = \Sigma\, a_j \mathbf{r}^{(j)}$$

where a_j is the magnitude of the component in the $\mathbf{r}^{(j)}$ direction (strength of the j^{th} wave, i.e., the jump in the characteristic variable across the interface). The interface flux difference can therefore be expressed as the composition of a collection of waves as follows:

$$d\mathbf{F} = \Sigma a_j b^{(j)} \mathbf{r}^{(j)} = d\mathbf{F}^+ + d\mathbf{F}^- = \Sigma^+ a_j b^{(j)} \mathbf{r}^{(j)} + \Sigma^- a_j b^{(j)} \mathbf{r}(j)$$

where $b^{(j)}$ is an eigenvalue of $\mathbf{A}$ (speed of j^{th} wave). Symbols Σ^+ and Σ^- denote summation over positive and negative wave speeds, respectively. The interface flux can therefore be computed from one of the following first-order expressions:

$$\mathbf{F}_{i+1/2} = \mathbf{F}_l + \Sigma^- a_j b^{(j)} \mathbf{r}^{(j)}$$

$$\mathbf{F}_{i+1/2} = \mathbf{F}_r - \Sigma^+ a_j b^{(j)} \mathbf{r}^{(j)}$$

$$\mathbf{F}_{i+1/2} = 1/2 \left[\mathbf{F}_l + \mathbf{F}_r - \Sigma a_j |b^{(j)}| \mathbf{r}^{(j)}\right]$$

The addition of a corrective flux to the previous formulae produces higher spatial accuracy flux-difference-splitting formulae. The family of these formulae is written as follows:

$$\mathbf{F}^{\wedge}_{i+1/2} = \mathbf{F}_{i+1/2} + (1+\Phi)/4(d\mathbf{F}^+_{i+1/2} - d\mathbf{F}^-_{i+1/2}) + (1+\Phi)/4(d\mathbf{F}^+_{i-1/2} - d\mathbf{F}^-_{i+3/2})$$

where the principal part of the truncation error is

$$(1/3 - \Phi)/4(\delta x)^2 \mathbf{F}_{,xxx}$$

APPENDIX C - FLUX LIMITERS

Total-variation-diminishing flux expressions make use of flux limiters. These limiters are generally made dependent on the values of a parameter ε proportional to the change in the characteristic variables across nearby interfaces:

$$\varepsilon^{(j)}_{i+*/2} = b^{(j)}_{i+*/2} a_{j\ i+*/2} = b^{(j)}_{i+*/2} l^{(j)}_{i+*2} \cdot df_{i+y*/2}$$

where $l^{(j)}$ is the left eigenvector of $\mathbf{A}$. The "minmod" limiter is defined as follows:

$$L_j(m,n) = \text{minmod}(\varepsilon^{(j)}_{i+m/2}, \beta\varepsilon^{(j)}_{i+n/2})$$

$$\text{minmod}(x,y) = \text{sign}(x)\max\{0, \min[|x|, y\text{sign}(x)]\}$$

where β is a compression parameter assumed to be equal to $(3 - \Phi)/(1 - \Phi)$. The "superbee" limiter is defined as follows:

$$L_j(m,n) = \text{cmplim}(\varepsilon^{(j)}_{i+m/2}, \varepsilon^{(j)}_{i+n/2})$$

$$\text{cmplim}(x,y) = \text{sign}(x)\max\{0, \min[|x|, \beta y\text{sign}(x)], \min[\beta|x|, y\text{sign}(x)]\}$$

where the compression parameter is now assumed to be β=2. The "van Leer" limiter is finally defined as follows:

$$L_j(m,n) = \text{vanlim}(\varepsilon^{(j)}_{i+m/2}, \varepsilon^{(j)}_{i+n/2})$$

$$\text{vanlim}(x,y) = (xy + |xy|)/(x + y)$$

REFERENCES

Dawes, W.N., 1986a, "Computation of Off-Design Flows in a Transonic Compressor Rotor," Journal of Engineering for Gas Turbines and Power, Vol. 108, No. 1, pp. 144-150.

Dawes, W.N., 1986b, "A Numerical Method for the Analysis of 3D Viscous Compressible Flow in Turbine Cascades; Application to Secondary Flow Development in a Cascade with and without Dihedral," ASME Paper 86-GT-145.

Dawes, W.N., 1987, "Application of a Three-Dimensional Viscous Compressible Flow Solver to a High Speed Centrifugal Compressor Rotor-Secondary Flow and Loss Generation," Turbomachinery - Efficiency Prediction and Improvement, Mechanical Engineering Publications, England, pp. 53-62.

Denton, J.D., 1983, "An Improved Time-Marching Method for Turbomachinery Flow Calculation," Journal of Engineering for Power, Vol. 105, No. 3, pp. 514-524.

Dring, R.P., Joslyn, H.D., Hardin, L.W., and Wagner, J.H., 1982, "Turbine Rotor-Stator Interaction," Journal of Engineering for Power, Vol. 104, No. 4, pp. 729-742.

Hah, C., 1984, "A Navier-Stokes Analysis of Three-Dimensional Turbulent Flows Inside Turbine Blade Rows at Design and Off-Design Conditions," Journal of Engineering for Power, Vol. 106, No. 2, pp. 421-429.

Hah, C., 1986, "A Numerical Modeling of Endwall and Tip-Clearance Flow of an Isolated Compressor Rotor," Journal of Engineering for Gas Turbines and Power, Vol. 108, No. 1, pp. 15-21.

Hathaway, M.D., 1986, "Unsteady Flows in a Single-Stage Transonic Axial-Flow Fan Stator Row," NASA TM-88929.

Hathaway, M.D., et al., 1987, "Measurements of the Unsteady Flow Field Within the Stator Row of a Transonic Axial-Flow Fan II - Results and Discussion," ASME Paper 87-GT-227. (Also, NASA TM-88946.)

Janus, J.M., 1989, "Advanced 3-D CFD Algorithm For Turbomachinery," Ph.D. Dissertation, Mississippi State University.

Moore, J., and Moore, J.G., 1985, "Performance Evaluation of Linear Turbine Cascades Using Three-Dimensional Viscous Flow Calculations," Journal of Engineering for Gas Turbines and Power, Vol. 107, No. 4, pp. 969-975.

Pierzga, M.J., and Wood, J.R., 1985, "Investigation of the Three-Dimensional Flow Field Within a Transonic Fan Rotor: Experiment and Analysis," Journal of Engineering for Gas Turbines and Power, Vol. 107, No. 2, pp. 436-449.

Roe, P.L., and Pike, J., 1984, "Efficient Construction and Utilization of Approximate Riemann Solutions," Computing Methods in Applied Sciences and Engineering 6, R. Glowinski and J.L. Lions, eds., North Holland, New York, pp. 499-518.

Roscoe, D.V., Shamroth, S.J., and McDonald, H., 1984, "An Ensemble Averaged Navier-Stokes Calculation Procedure for the Prediction of Two- and Three-Dimensional Radial Diffuser Flow Fields," Computational Methods in Turbomachinery, Mechanical Engineering Publications, England, pp. 67-76.

Shamroth, S., McDonald, H., and Briley, W.R., 1982, "Application of a Navier-Stokes Analysis to Transonic Cascade Flow Fields," ASME Paper 82-GT-235.

Steger, J.L., and Warming, R.F., 1979, "Flux Vector Splitting of the Inviscid Gasdynamic Equations with Application to Finite Difference Methods," NASA TM-78605.

Suder, K.L., et al., 1987, "Measurements of the Unsteady Flow Field Within the Stator Row of a Transonic Axial-Flow Fan I - Measurement and Analysis Technique," ASME Paper 87-GT-226. (Also, NASA TM-88945.)

Van Hove, W., 1984, "Calculation of Three Dimensional Inviscid Rotational Flow in Axial Turbine Blade Rows," Journal of Engineering for Gas Turbines and Power, Vol. 106, No. 2, pp. 430-436.

Weinberg, B.C., Yang, R.J., McDonald, H., and Shamroth, S.J., 1986, "Calculations of Two- and Three-Dimensional Transonic Cascade Flow Fields Using the Navier-Stokes Equations," Journal of Engineering for Gas Turbines and Power, Vol. 108, No. 1, pp. 93-102.

Whitfield, D.L., and Janus, J.M., 1989, "A Simple Time-Accurate Turbomachinery Algorithm with Numerical Solutions of an Uneven Blade Count Configuration," AIAA Paper 89-0206.

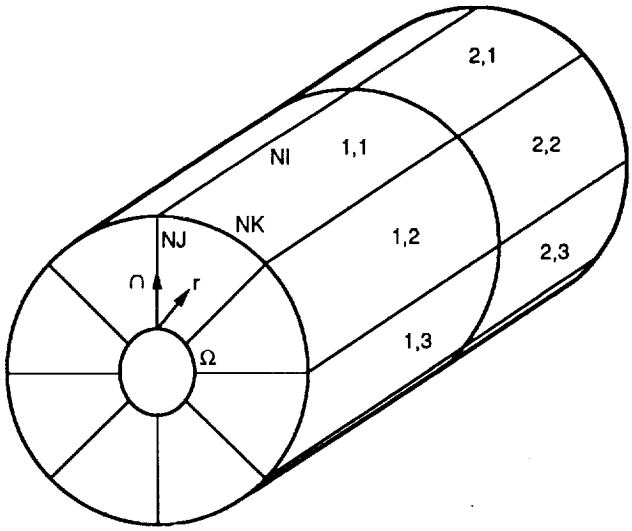

Figure 1.—Axial and circumferential partition of the flow domain.

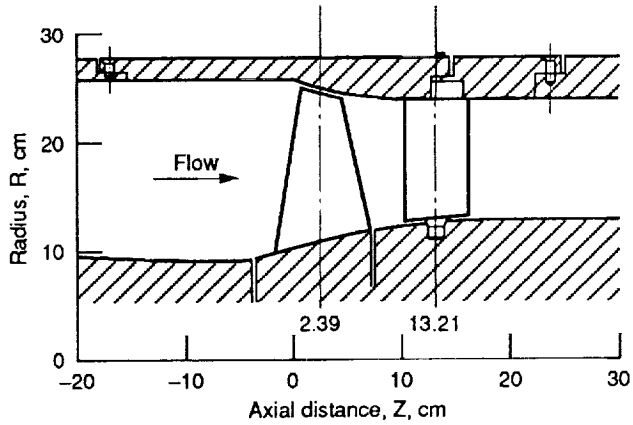

Figure 2.—Meridional plane view.

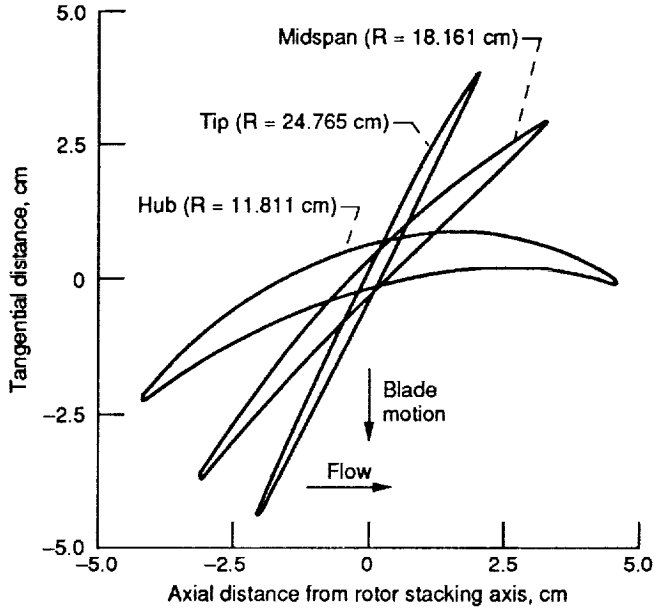

Figure 3.—Rotor blade sections.

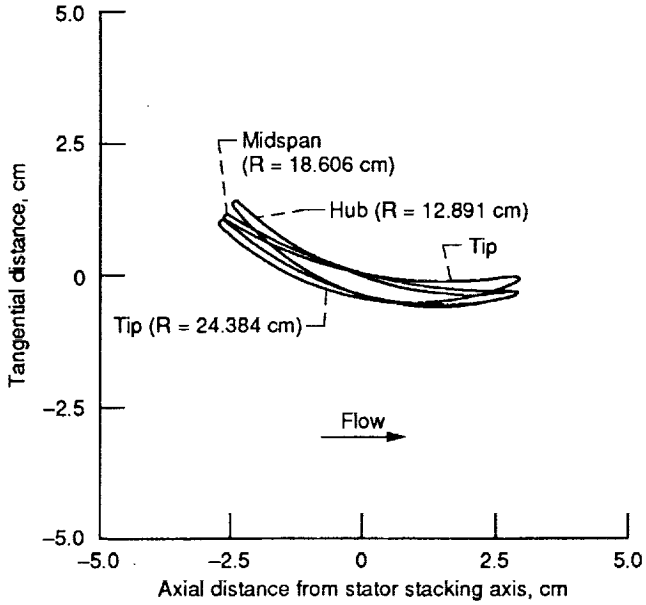

Figure 4.—Stator blade sections.

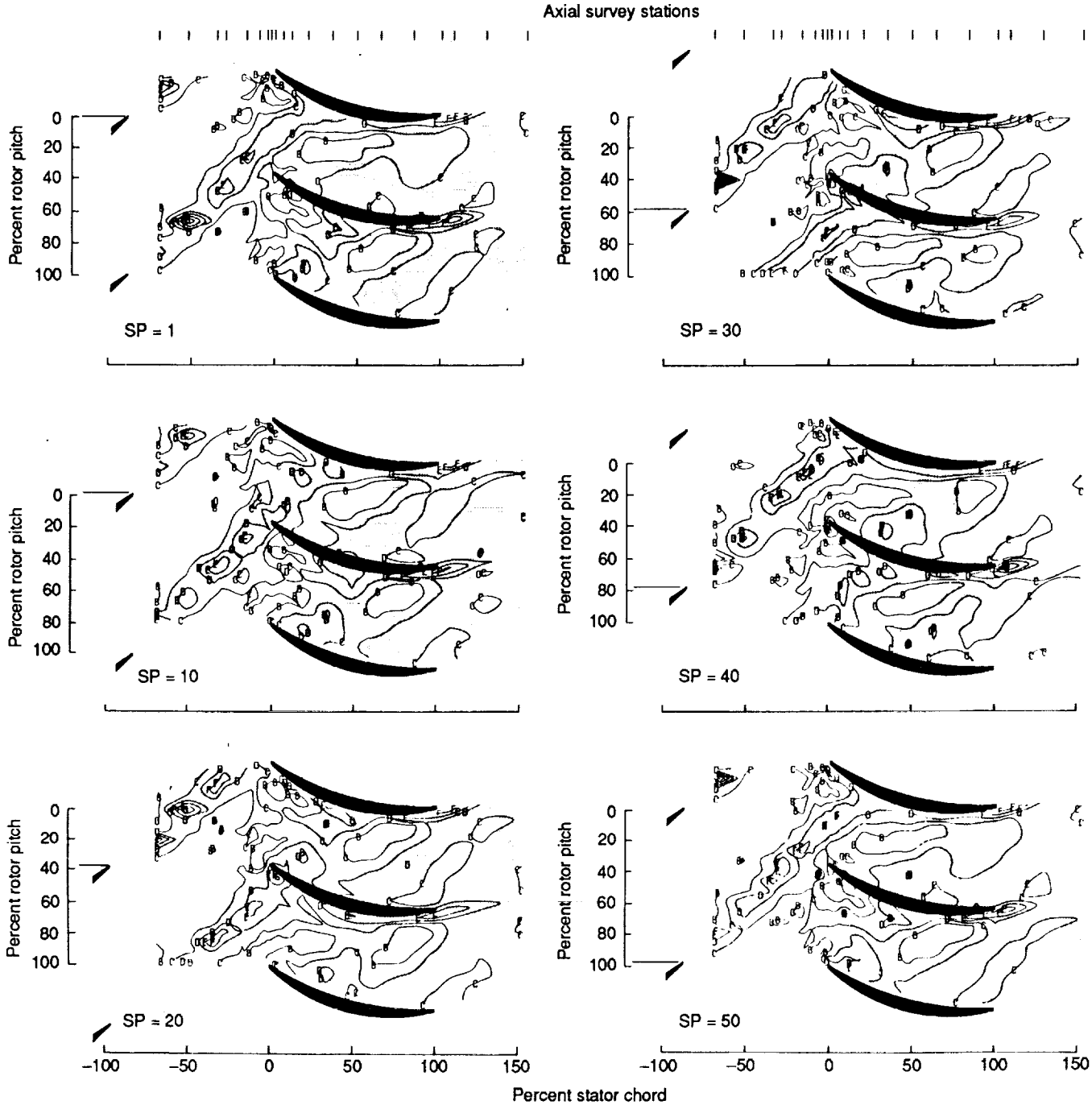

Figure 5.—Experimental turbulence kinetic energy contours within the stator row at different rotor shaft positions (Hathaway et al., 1987).

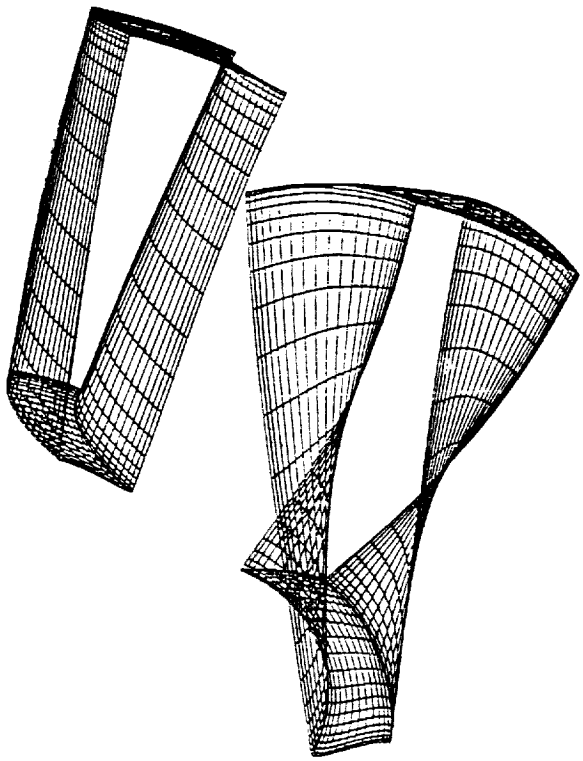

Figure 6.—Rotor and stator blade passage computational grids.

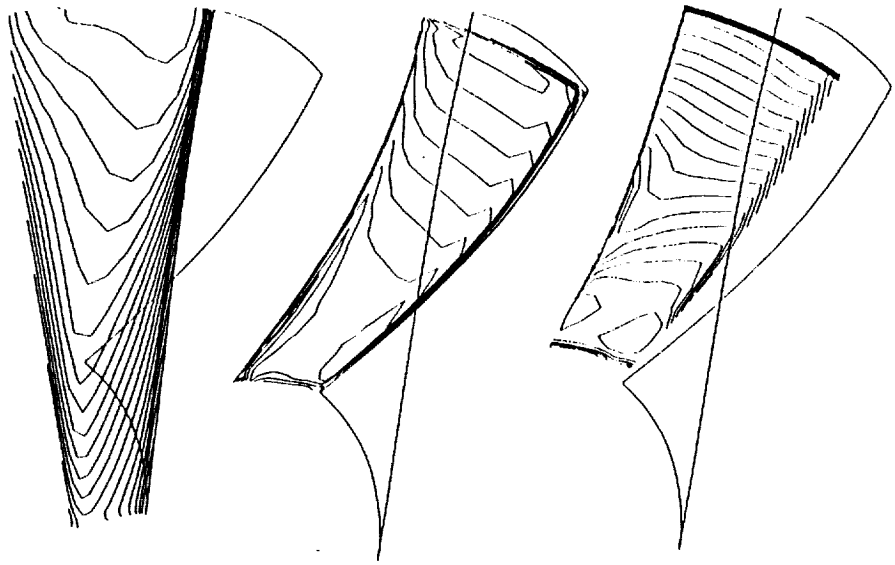

Figure 7.—Theoretical (present code) relative Mach number contours in the leading edge, trailing edge, and outlet plane of the rotor row (results obtained with downstream stator row).

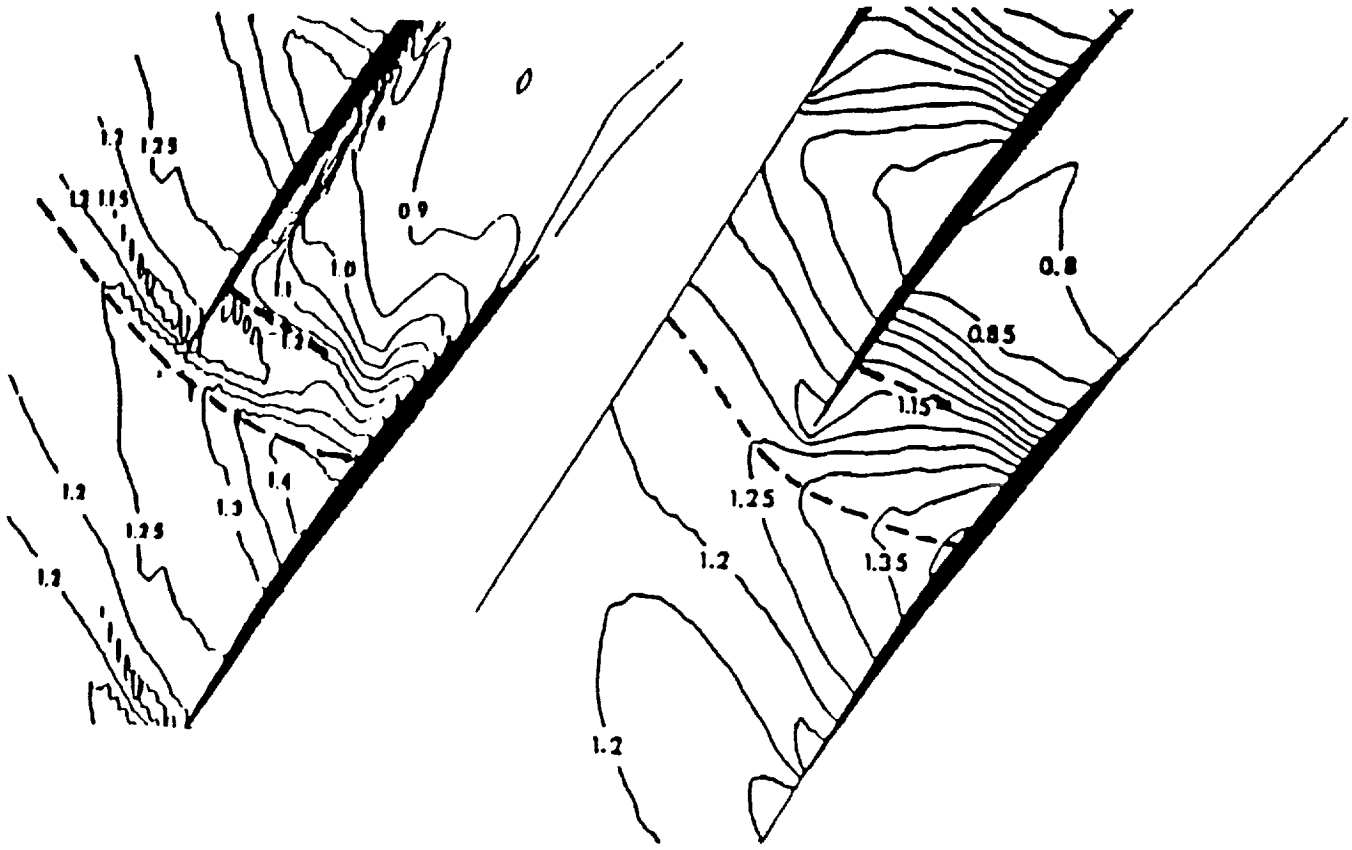

Figure 8.—Experimental (left) and theoretical (Denton's code, right) relative Mach number contours in rotor row at 30-percent span from the tip (Pierzga and Wood, 1985, results obtained without downstream stator row).

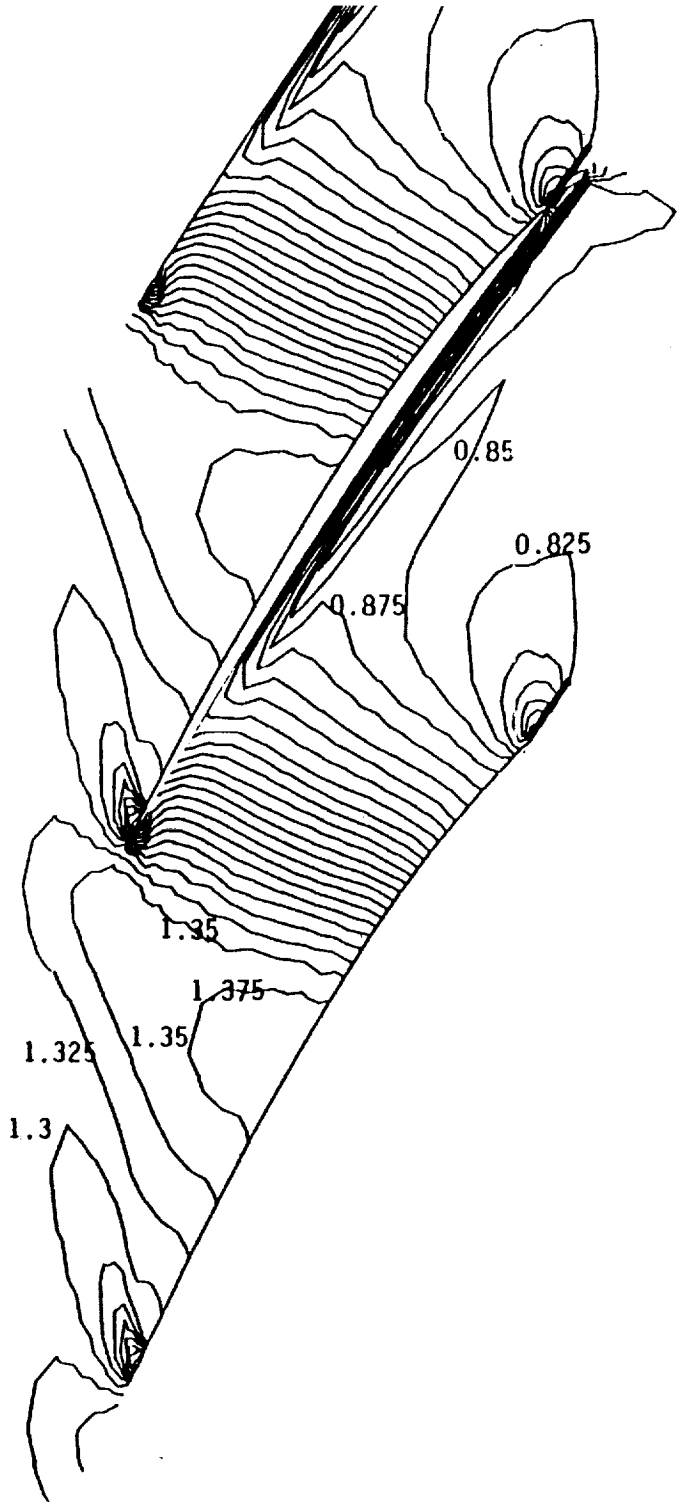

Figure 9.—Theoretical (present code) relative Mach number contours in rotor row at 30-percent span from tip (results obtained with downstream stator row).

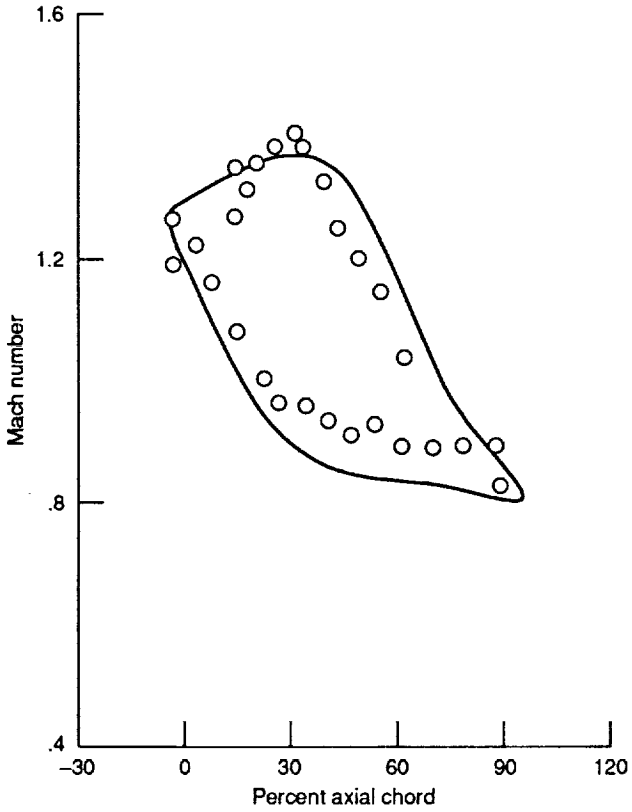

Figure 10.—Comparison between theoretical (present code, results obtained with a downstream stator row) and experimental (Pierzga and Wood, 1985, results obtained without a downstream stator row) blade relative Mach number distributions in the rotor row at 30-percent span from the trip.

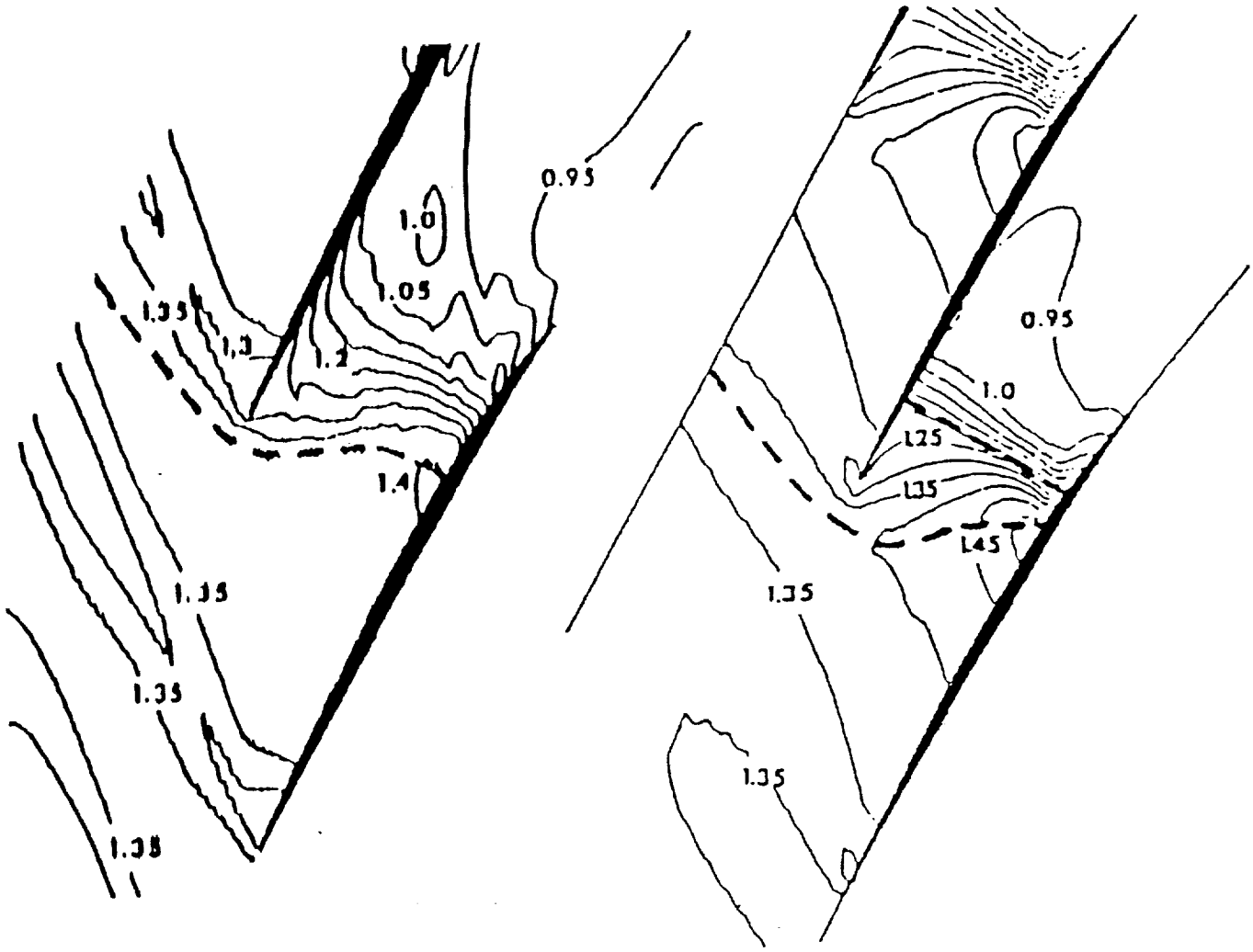

Figure 11.—Experimental (left) and theoretical (Denton's code, right) relative Mach number contours in rotor row at 10-percent span from tip (Pierzga and Wood, 1985, results obtained without downstream stator row).

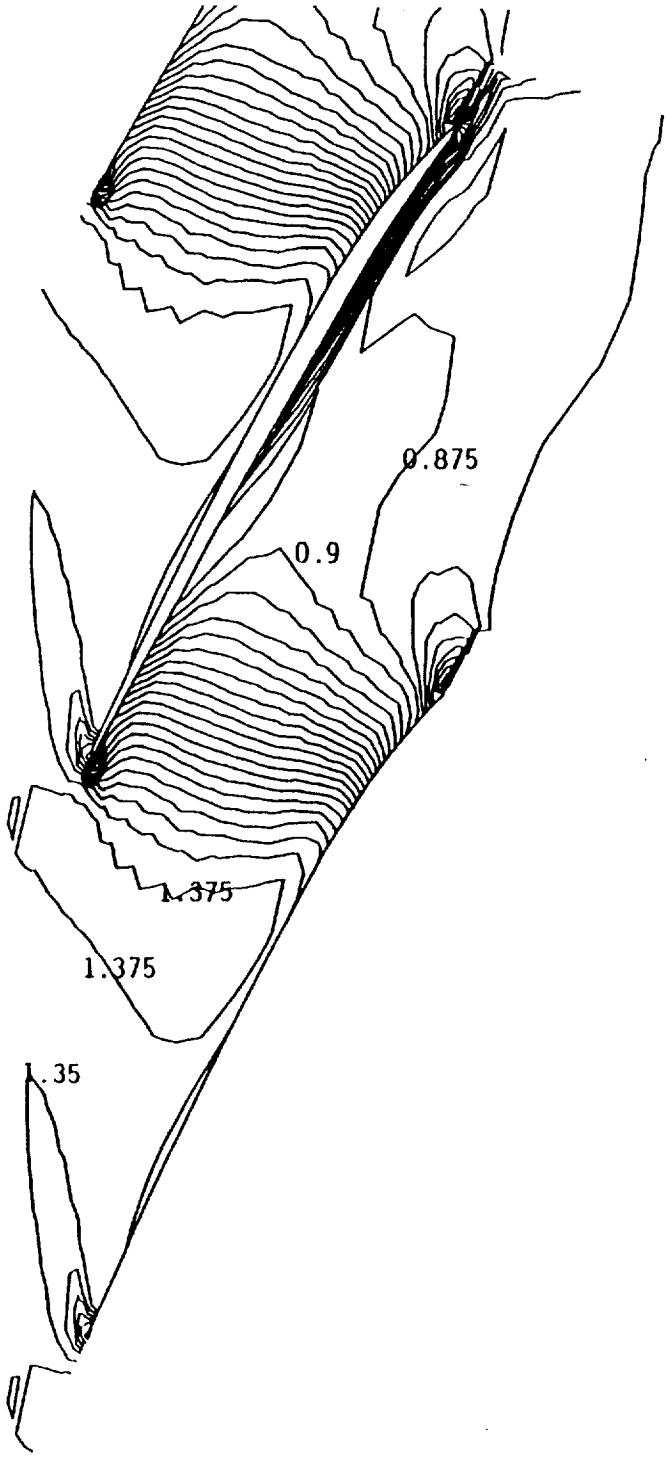

Figure 12.—Theoretical (present code) relative Mach number contours in rotor row at 10-percent span from tip (results obtained with downstream stator row).

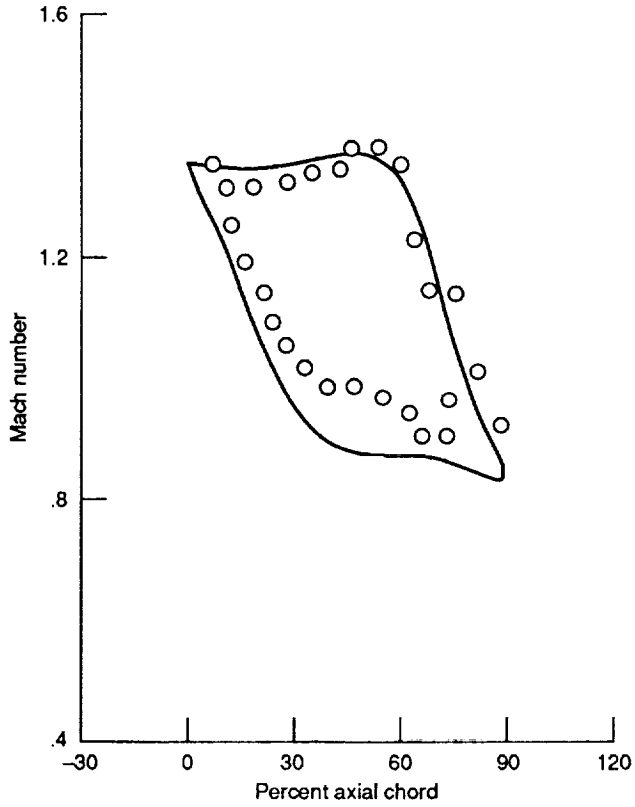

Figure 13.—Comparison between theoretical (present code, results obtained with a downstream stator row) and experimental (Pierzga and Wood, 1985, results obtained without a downstream stator row) blade relative Mach number distributions in the rotor row at 10-percent span from the trip.

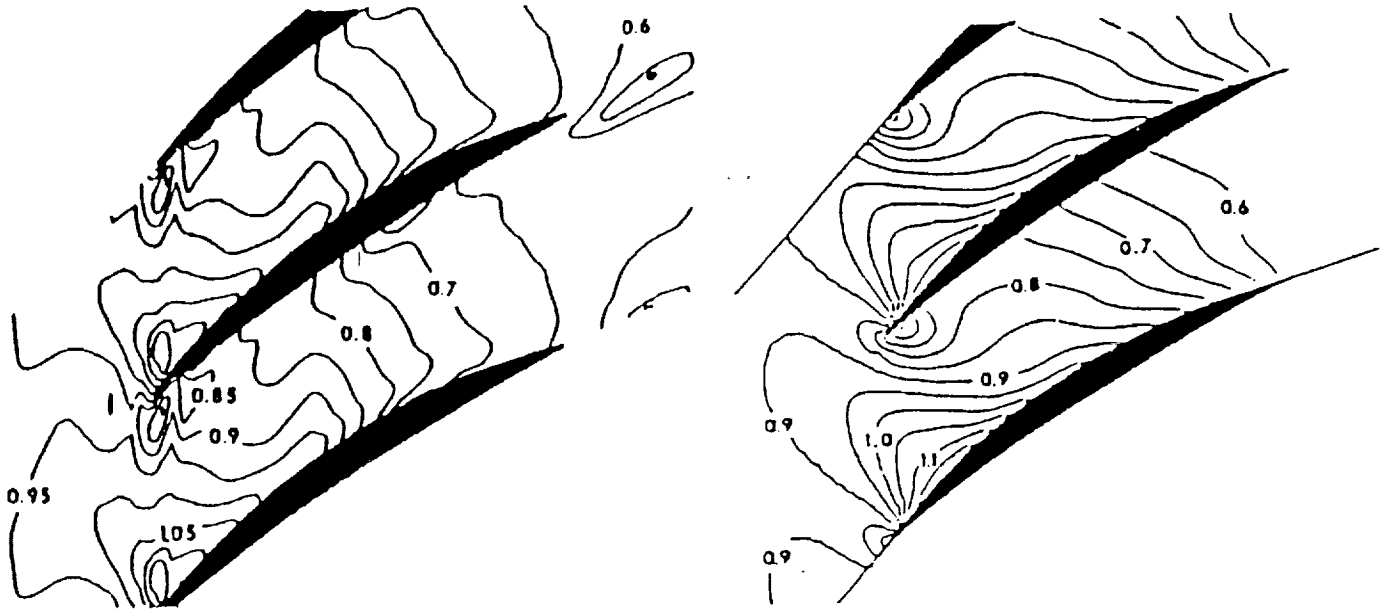

Figure 14.—Experimental (left) and theoretical (Denton's code, right) relative Mach number contours in rotor row at 70-percent span from tip (Pierzga and Wood, 1985, results obtained without downstream stator row).

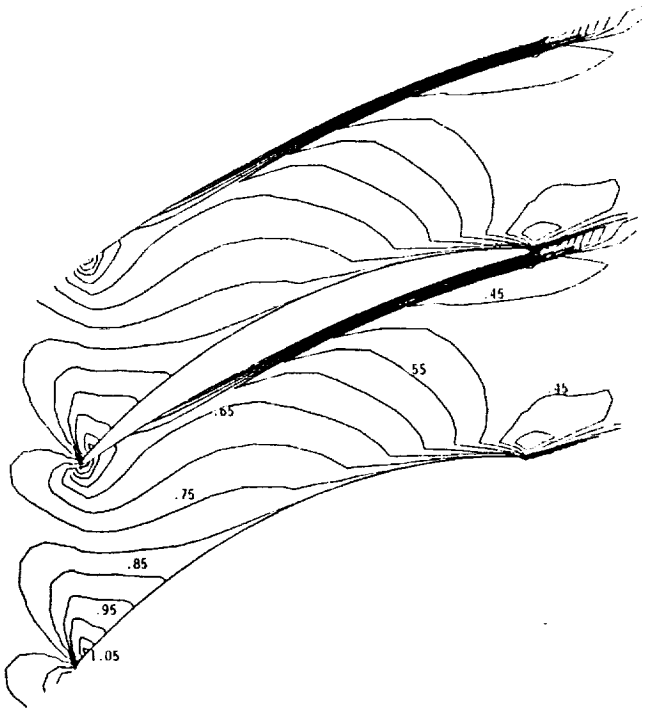

Figure 15.—Theoretical (present code) relative Mach number contours in rotor row at 70-percent span from tip (results obtained with downstream stator row).

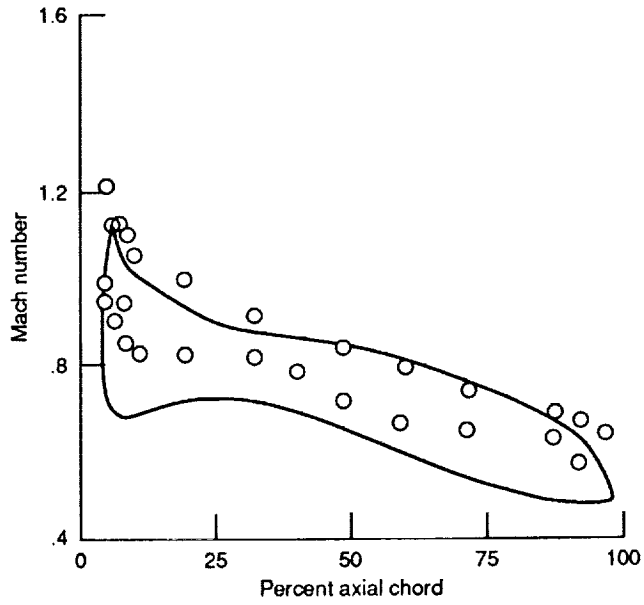

Figure 16.—Comparison between theoretical (present code, results obtained with a downstream stator row) and experimental (Pierzga and Wood, 1985, results obtained without a downstream stator row) blade relative Mach number distributions in the rotor row at 70-percent span from the trip.

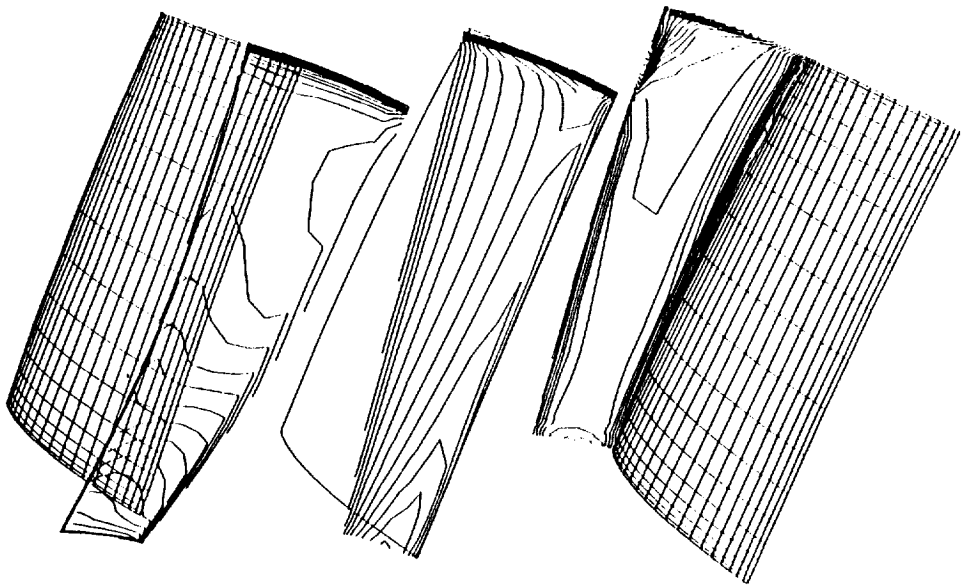

Figure 17.—Theoretical (present code) Mach number contours in the inlet, leading edge, and trailing edge planes of the stator row (results obtained with an upstream rotor row).

Line	Mach number
G	0.47
H	.50
I	.53
J	.56
K	.59
L	.62
M	.65
N	.68
O	.71
P	.74
Q	.76
R	.79

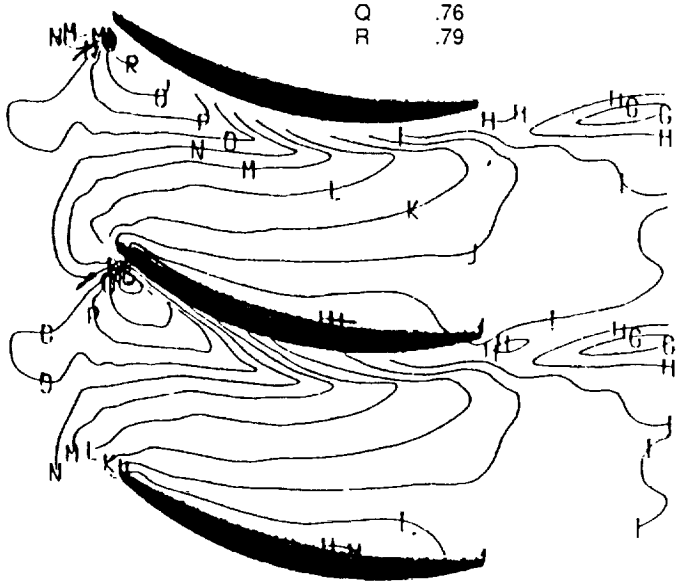

Figure 18.—Experimental Mach number contours in stator row at 50-percent span from tip (Hathaway et al., 1987, results obtained with an upstream rotor row).

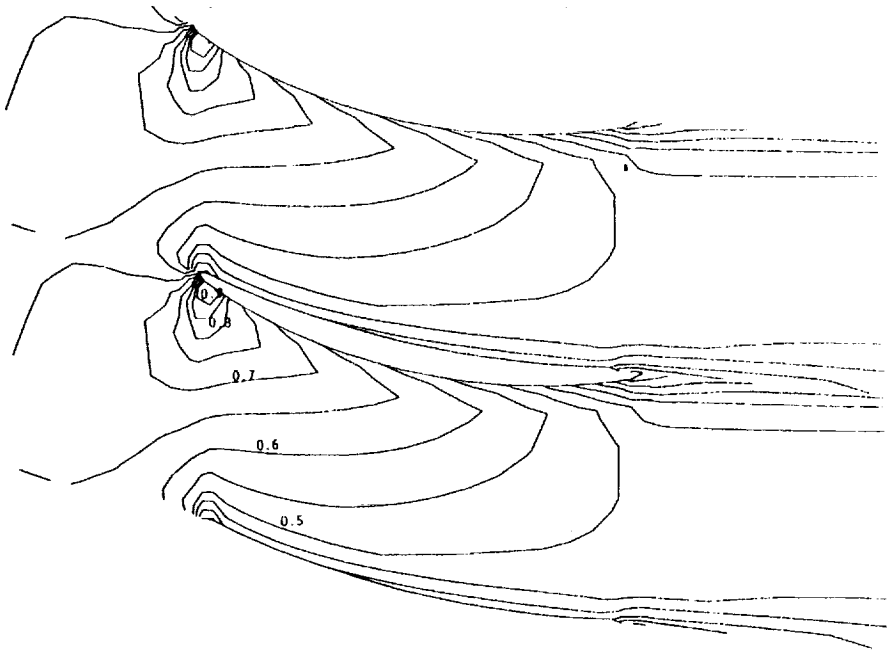

Figure 19.—Theoretical (present code) Mach number contours in stator row at 50-percent span from tip (results obtained with an upstream rotor row).

NASA
National Aeronautics and Space Administration

Report Documentation Page

1. Report No.	2. Government Accession No.	3. Recipient's Catalog No.
NASA TM-102528 ICOMP-90-08		

4. Title and Subtitle	5. Report Date
Three-Dimensional Euler Time Accurate Simulations of Fan Rotor-Stator Interactions	December 1990
	6. Performing Organization Code

7. Author(s)	8. Performing Organization Report No.
A.A. Boretti	E-5338
	10. Work Unit No.
	505-62-21

9. Performing Organization Name and Address	11. Contract or Grant No.
National Aeronautics and Space Administration Lewis Research Center Cleveland, Ohio 44135-3191	
	13. Type of Report and Period Covered
	Technical Memorandum

12. Sponsoring Agency Name and Address	14. Sponsoring Agency Code
National Aeronautics and Space Administration Washington, D.C. 20546-0001	

15. Supplementary Notes

A.A. Boretti, Sistemi Elettronici Tecniche di Controllo, Centro Ricerche FIAT—MOTORI, Orbassano, Italy, and Institute for Computational Mechanics in Propulsion, Lewis Research Center (work funded by Space Act Agreement C-99066-G). Space Act Monitor: Louis A. Povinelli (216) 433-5818.

16. Abstract

The paper presents a numerical method useful to describe unsteady three-dimensional flow fields within turbomachinery stages. The method solves the compressible, time-dependent, Euler conservation equations with a finite-volume, flux-splitting, total-variation-diminishing, approximately factored, implicit scheme. Multiblock composite gridding is used to partition the flow field into a specified arrangement of blocks with static and dynamic interfaces. The code is optimized to take full advantage of the processing power and speed of the Cray Y/MP supercomputer. The method is applied to the computation of the flow field within a single-stage, axial flow fan, thus reproducing the unsteady three-dimensional rotor-stator interaction.

17. Key Words (Suggested by Author(s))	18. Distribution Statement
Euler equations Unsteady internal flows Time-accurate simulation	Unclassified – Unlimited Subject Category 02

19. Security Classif. (of this report)	20. Security Classif. (of this page)	21. No. of pages	22. Price*
Unclassified	Unclassified	30	A03

NASA FORM 1626 OCT 86

*For sale by the National Technical Information Service, Springfield, Virginia 22161